

Creep Resistance and Fracture Toughness of Recently-Developed Optimized Grade 92 and Its Weldments for Advanced Fast Reactors[†]

L. Tan¹, M.A. Sokolov¹, T.-L. Sham²

¹Oak Ridge National Laboratory (ORNL), Oak Ridge, Tennessee, USA

²Argonne National Laboratory (ANL), Lemont, Illinois, USA

E-mail contact of main author: tanl@ornl.gov

Abstract. Optimized Grade 92 (Opt.G92) has been developed at Oak Ridge National Laboratory in support of the USA Sodium-cooled Fast Reactor program. Composition modification and processing optimization successfully achieved the development of Opt.G92 with desired microstructures for superior properties. A variety of properties have been assessed for Opt.G92, which include tensile, creep, fatigue, creep-fatigue, impact and fracture toughness, weldability, thermal aging resistance, and sodium compatibility. This paper focuses on presenting the results of creep and fracture toughness tests of Opt.G92 and its weldments. Compared to the literature data of Grade 92, Opt.G92 exhibited moderate enhancement in creep resistance, together with superior or comparable fracture toughness. Creep rupture ductility of the ruptured specimens is discussed by comparing to the reference steels. Creep tests of Opt.G92 at 650°C are ongoing and they will provide data to assess if creep rupture ductility will deteriorate at lower stresses as the case for Grade 92. Specimens extracted from tungsten-inert-gas fabricated weldments showed some reductions in creep life and creep strength compared to the base metal of Opt.G92, approximately following the trends of the weldments and base metal of Grade 92, but with greater creep life and strength. Satisfactory fracture toughness was observed for the weldments and base metal of Opt.G92. Microstructural characterization following the tests shed light on the superior properties of Opt.G92 and its weldments.

Key Words: Larson-Miller parameter, creep rupture ductility, microstructure, Laves phase.

1. Introduction

For the large-scale industrial deployment of advanced fast reactors, there must be improvements in the capital cost and economic return of such reactors. Further, greater safety margins and increased design flexibility will also be important for any new system. Flexibility, safety, and economics have been identified as key needs for advanced nuclear reactors. Advanced materials play an important role in fulfilling these needs. Improved structural material performance is one way to improve the economics of fast reactors, by potentially allowing both higher operating temperatures (and thus, higher thermal efficiency and power output) and longer lifetimes for components. Improved materials reliability could also reduce reactor down time. Superior structural materials will also spur improvements in high temperature design methodology and thereby allow more flexibility in construction and operation.

[†] The United States Government retains and the publisher, by accepting the article for publication, acknowledges that the United States Government retains a non-exclusive, paid-up, irrevocable, world-wide license to publish or reproduce the published form of this manuscript, or allow others to do so, for United States Government purposes. The Department of Energy will provide public access to these results of federally sponsored research in accordance with the DOE Public Access Plan (<http://energy.gov/downloads/doe-public-access-plan>).

Ferritic-martensitic steel Grade 92 (9Cr-2WMoVNb or T/P92 in the ASTM A213/A335) was selected for further development as part of the U.S. Sodium-cooled Fast Reactor (SFR) program because the base alloy offer considerable improvements in strength and creep resistance over more mature steel, such as Grade 91 (Mod. 9Cr-1Mo or 9Cr-1MoVNb or T/P91 in the ASTM A213/A335). Despite the recent successful development of high-Co/W alloyed 9Cr ferritic-martensitic steels that exhibit significantly enhanced creep resistance compared to Grade 92 [1,2], they are not applicable to nuclear applications due to their Co content. As a result, developmental efforts have been focused on advanced 9Cr FM steels that can be deployed in SFRs.

The development of optimized Grade 92 (Opt.G92) was pursued by two routes. Steel composition basically followed the ASTM specification of Grade 92 with tighter control of chemistry, together with optimization of some alloying elements after comprehensive literature reviews on the effects of alloying elements on mechanical properties of 9–12 wt% Cr ferritic-martensitic steels, e.g., greater content of Ni, Si, and Mn leading to decreased strength [3,4]. Following previous successful practices on 9 wt% Cr ferritic-martensitic steels [5,6,7], thermomechanical treatments were explored on the new steels by forgoing and/or rolling at different temperature regimes to obtain Opt.G92 for test in this work. Computation thermodynamics using the Calphad approach has guided steel composition adjustment as well as processing temperatures.

Creep resistance and fracture toughness are two of the essential properties that determine a component's lifetime and design safety margins. This paper reports the collected results of these two properties for both base metal (BM) and weldments of Opt.G92, which are compared to the literature data of Grade 92.

2. Material and Testing

Six heats of Opt.G92 in a forged plate product form were procured from an U.S. commercial steel manufacturer. The heats were melted by either vacuum induction melting (VIM) plus electro-slag remelting (ESR) or VIM only. The use of ESR resulted in slight composition changes to a few alloying elements such as nitrogen, silicon, and niobium and impurity of copper [8,9]. Four of the heats, two VIM+ESR and two VIM, have been used for creep and fracture toughness tests following respective ASTM standard test methods. Weldments were prepared by the commonly used tungsten inert gas welding technique with standard commercial filler metal for Grade 92.

Standard creep specimens with a gauge section of 6.35 mm diameter (D) and 31.75 mm length (L) were tested in air at 550, 600, and 650°C and a variety of loads for the BM. A longer gauge length of 57.15 mm with the same gauge diameter ($L/D = 9$) was used for cross-welds specimens, tested in air at 650°C and loads of 90 and 100 MPa. The gauge section of all the creep specimens was aligned with the longitudinal direction of the plates.

Standard ASTM 0.5T compact tension (CT) specimens were used for fracture toughness tests in air in the ductile to brittle transition region as well as in the ductile region at elevated temperatures. The 0.5T CT specimens were extracted along the transverse–longitudinal orientation of the BM, but along the weld line in the longitudinal–transverse orientation of the weldments.

Microstructural characterization of the tested specimens was conducted using optical microscopy, scanning electron microscopy (SEM: JEOL 6500 field-emission gun), and energy dispersive X-ray spectroscopy (EDS: EDAX Silicon Drift Detector).

3. Results and Discussion

2.1. Creep Resistance

The representative creep curves with stress as a function of creep time are shown in Fig. 1 for the Opt.G92 specimens tested at 550, 600, and 650°C and loads of 260, 180, and 100 MPa, respectively. The curves show classic primary, secondary, and tertiary creep stages. The photos of the respective ruptured specimens are shown as inset of Fig. 1, showing pronounced necking in the gauge section at creep rupture.

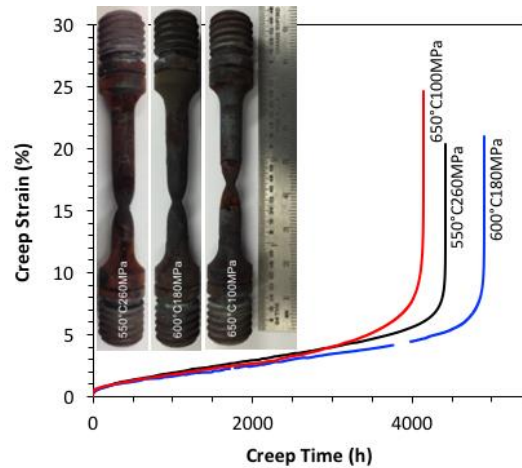


FIG. 1. Representative creep curves and respective photos of the creep-ruptured Opt.G92 specimens tested at 550, 600, and 650°C.

Larson-Miller equation is used to plot and analyze the creep data with Larson-Miller parameter $P = T(C_{LM} + \log t_r)$, where C_{LM} is the Larson-Miller constant setting to 35.28 for comparison purpose [10], T is the temperature in Kelvin, and t_r is the time to rupture in hour. Using the data, log-stress values are fit with a fourth order polynomial in P . Figure 2 exhibits the data of Opt.G92 in red diamonds, compared to the literature data of Grade 92 [11] in black triangles. The few data attached with arrows indicate the ongoing tests of Opt.G92 specimens. The results indicate that Opt.G92 has a significant improvement in the high-stress regime above ~200 MPa, and a moderate improvement at lower stresses of creep resistance compared to Grade 92.

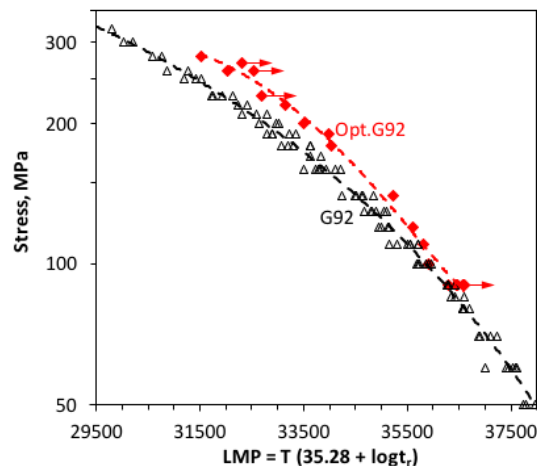


FIG. 2. Stress as a function of the Larson-Miller parameter of the creep-ruptured Opt.G92 compared to the literature data of Grade 92 [11].

Ferritic-martensitic steels generally suffer from low creep rupture ductility failure at higher temperatures and lower stresses. Grade 92 had more reports of low creep rupture ductility failure than Grade 91. Figure 3 plots Grade 92 data with area of reduction of creep-ruptured specimens as a function of stress [11,12,13,14]. Only the 650°C data are plotted here because pronounced decreases of area of reduction with stress reduction (as indicated by the shaded thick bar) occur when the stresses are below a critical value of ~110 MPa for T92 at 650°C. Such creep-rupture ductility reduction is minor for reported tests at lower temperatures. The tube form product (e.g. MJT and T92) generally had lower area of reduction than the pipe form (e.g., MJP and P92) at the same temperature and stress. Analyses indicated that the low creep rupture ductility failure may have been caused by the larger amount of inclusions, e.g., MnS and Al₂O₃, in the P92 induced by its high impurity content of sulfur (0.006 wt%) and aluminum (0.005 wt%) [13]. Area of reduction does not follow the decreasing trend of the shaded thick bar when area of reduction is < ~10% with stress < 90 MPa at 650°C.

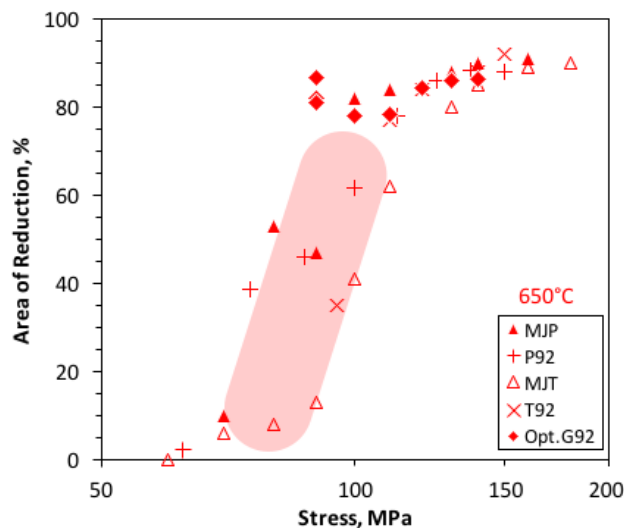


FIG. 3. Stress-dependent creep rupture ductility (area of reduction) of Opt.G92 compared to the literature data of Grade 92 [11,12,13,14].

The stress-dependent area of reduction of Opt.G92 specimens tested at 650°C is plotted in Fig. 3 in red diamonds. The results of the creep-ruptured specimens are comparable to the pipe form product of the literature data at temperatures above 100 MPa. The completed three tests at 90 MPa and 650°C exhibited significantly greater area of reduction than the literature data, suggesting improved creep rupture ductility of Opt.G92. The ongoing additional tests at 90 MPa and 650°C will provide further evidence of Opt.G92 superior to Grade 92 in terms of creep rupture ductility.

Figure 4 shows SEM images in backscattered electron mode (a-d) and secondary electron mode (e), illustrating the typical microstructures developed at the tab, gauge, necking, and rupture sites at 650 and 550°C. Other than the sizes and number densities of Laves phase, the test at 650°C and 120 MPa (Fig. 4b) did not result in much changes in the microstructures at the tab section compared to the gauge section of the test at 550°C and 260 MPa (Fig. 4d). However, nearly complete recrystallization occurred at the necking site of the test at 650°C and 120 MPa (Fig. 4a), compared with the necking site of the test at 550°C and 260 MPa (Fig. 4c) having partial recrystallization embedded in the overall much finer microstructure elongated along load direction. The recrystallization would decrease strength and alter

ductility. The effect of such recrystallization on creep rupture ductility needs to be investigated. Figure 4e exhibits many cavities at the ruptured site of the test at 550°C and 260 MPa, most of which were associated with oxide particles enriched with (Cr,Mn,V). This type of inclusions was also observed in the gauge and tab sections of the tested specimens, which is different from the generally observed inclusions in Grade 92, such as MnS, Al₂O₃, and BN, resulting in low creep rupture ductility [13]. The formation of the complex (Cr,Mn,V) oxide inclusions and their effect on creep rupture ductility are need to be investigated.

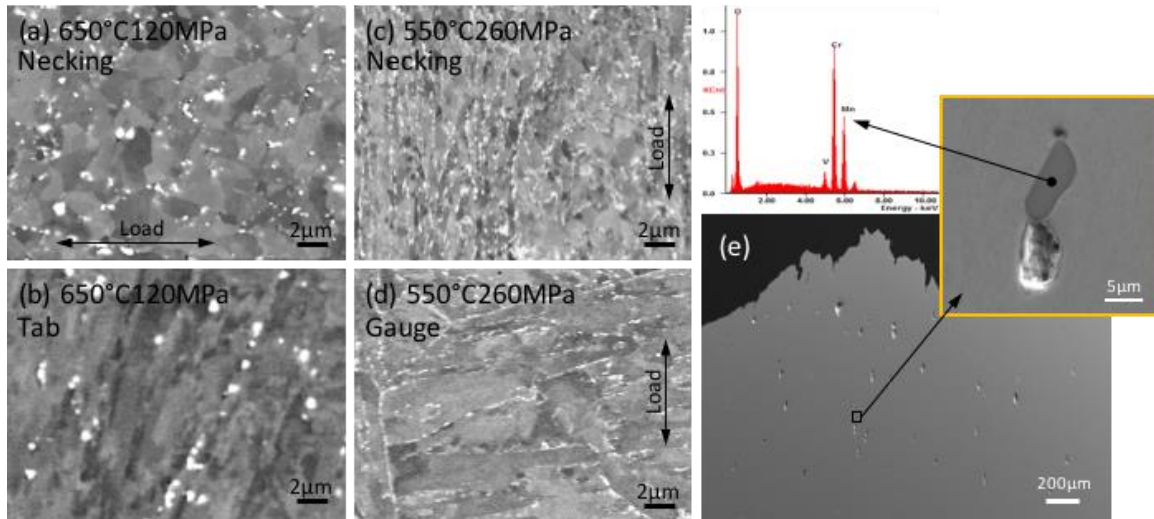


FIG. 4. Typical microstructures of the creep-ruptured specimens of Opt.G92 tested at (a, b) 650°C, (c, d) 550°C, and (e) cavities at the ruptured site of (c).

A few cross-welds specimens of Opt.G92 were tested at 100 and 90 MPa at 650°C. Two data at 100 MPa and one datum at 90 MPa are shown in Fig. 5 with stress as a function of time to rupture. The results of Opt.G92 BM with the ongoing tests at 90 MPa (with an arrow), as well as the cross-welds and BM of Grade 92 [15], are included in Fig. 5 for comparison. In general, the limited cross-welds results suggest that both the cross-welds and BM of Opt.G92 approximately follow the trends of the cross-welds and BM of Grade 92, and shift to greater time to rupture.

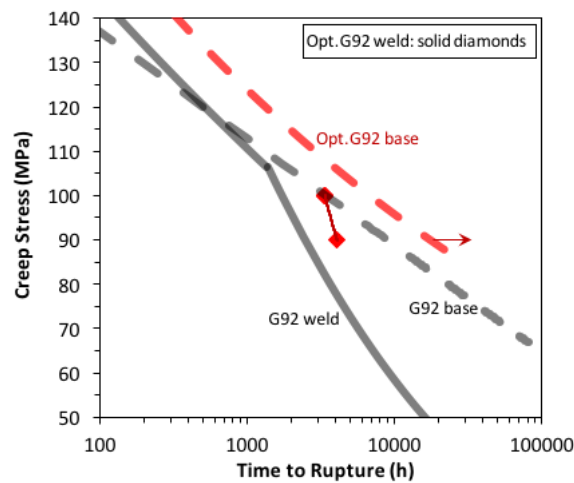


FIG. 5. Cross-welds creep resistance of Opt.G92 compared to the literature data of Grade 92 at 650°C [15].

The microstructures of a cross-welds specimen tested at 650°C and 100 MPa are shown in Fig. 6. The overall optical image (Fig. 6a) exhibits weld metal (WM) between the two heat-affected zones (HAZ) outlined by two white dashed parallelograms, together with the BM on the left end. The specimen ruptured within the right HAZ, close to the BM-HAZ interface, which indicates type-IV cracking of the specimen with a decent area of reduction of ~30%. A series of SEM images in the BSE mode were taken across the left HAZ, as well as the tab, shoulder, and the ruptured right HAZ of the specimen. Figure 6b shows an example of such images, illustrating Laves phase particles in white and cavities in dark. Image analyses for the Laves phase and cavities were conducted on the collected BSE images. The results are plotted in Fig. 6c-d with area% and average size of the Laves phase and cavities as a function of distance at different locations. It indicates that cavities and Laves phase have a strong relationship between their area%, but not between their average sizes. The moderately increased amount of Laves phase in the WM, which may be resulted from the higher Mo content of the filler metal than the BM and the coarse grain structures of the WM, did not result in noticeable increases in the area% of cavities. It is unclear why the cavities and Laves phase in the ruptured right HAZ do not follow the same relationship in the left HAZ, which has the largest amount of cavities but with approximately the least amount of Laves phase. The fate of the Laves phase at the rupture site during the later stage of creep tests needs to be investigated.

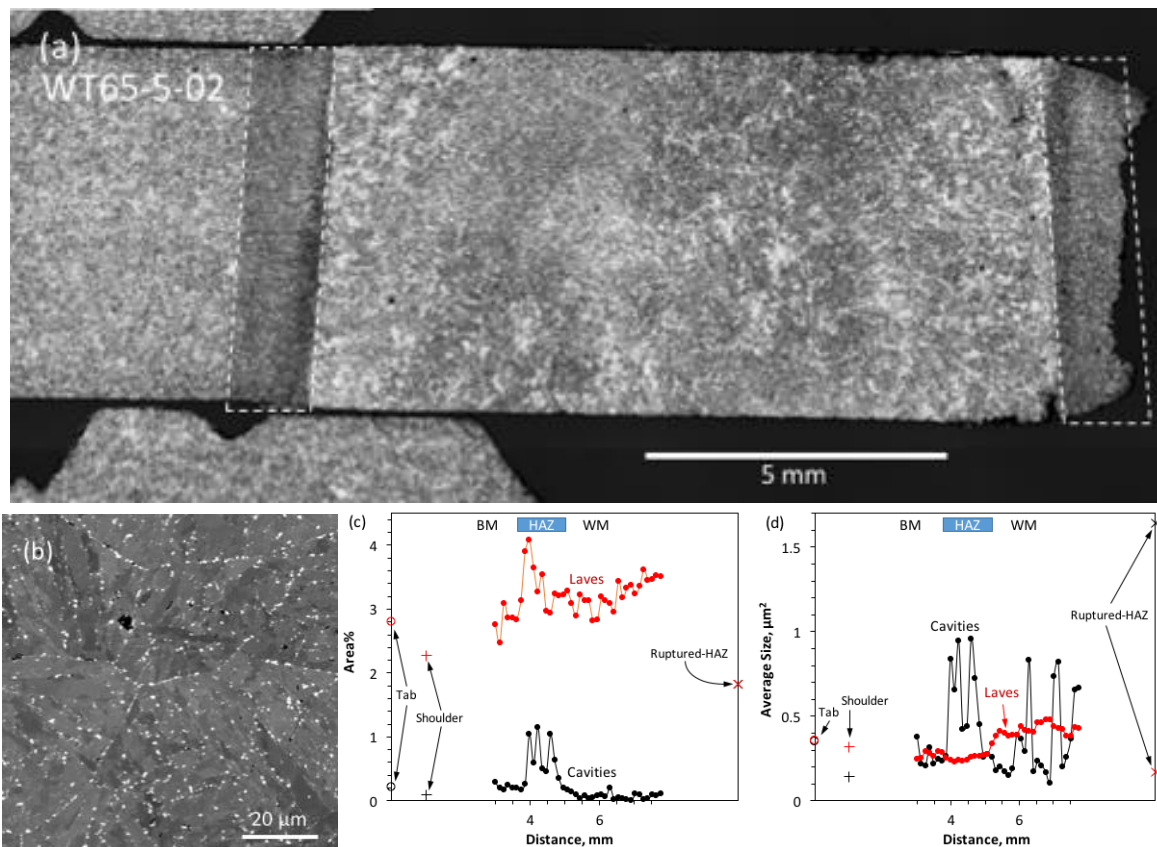


FIG. 6. Microstructural analyses of the creep-ruptured cross-welds: (a) overview micrograph including the retained left HAZ and the ruptured right HAZ, (b) typical BSE image showing Laves phase and cavities, (c, d) analyzed area% and average size of Laves phase and cavities across the left HAZ compared to that at tab, shoulder and ruptured right HAZ.

2.2. Fracture Toughness

Fracture toughness results in the transition and ductile regions of Opt.G92 and its weldments are plotted in Fig. 7a and 7b, respectively. The two heats of Opt.G92, i.e., G92-4T in black diamonds and curves and G92-8T in red squares and curves, showed about the same results in the transition region with $T_0 = -34^\circ\text{C}$ in Fig. 7a. The WM of Opt.G92 exhibited lower toughness with $T_0 = -17^\circ\text{C}$. In the ductile region at elevated temperatures, Opt.G92 (heat G92-9T) showed about constant toughness of $201 \pm 25 \text{ MPa}\sqrt{\text{m}}$, in contrast to the decreased toughness with higher temperature to $\sim 132 \text{ MPa}\sqrt{\text{m}}$ at $500\text{--}650^\circ\text{C}$. Slightly greater toughness of $260 \pm 27 \text{ MPa}\sqrt{\text{m}}$ and comparable toughness of $209 \pm 28 \text{ MPa}\sqrt{\text{m}}$ were observed in the WM (heat G92-4T) and HAZ (heat G92-9T), respectively, compared to Opt.G92 at $500\text{--}650^\circ\text{C}$.

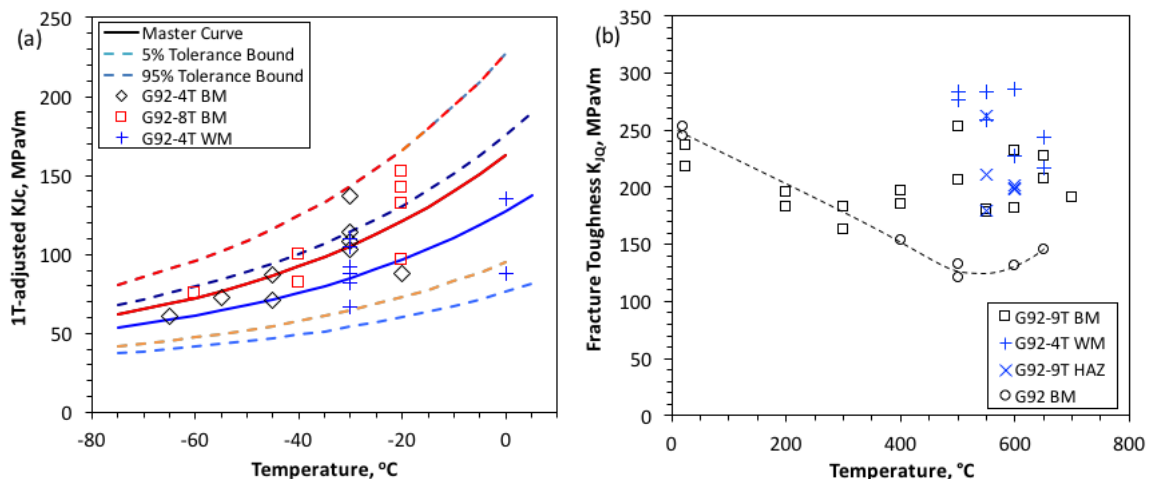


FIG. 7. Fracture toughness of Opt.G92 and its welds in the (a) transition and (b) ductile regions.

4. Conclusion

Four heats of Opt.G92 were developed and evaluated by creep and fracture toughness tests in this work. Compared to literature data of Grade 92, Opt.G92 exhibited moderate enhancement in creep resistance for the tests conducted at 550 , 600 , and 650°C in air. The tested specimens had excellent creep rupture ductility comparable to Grade 92 at the similar conditions. The significantly refined grains by recrystallization in the necking area may have benefited high creep rupture ductility. The ongoing creep tests of Opt.G92 at 650°C will provide evidence to assess if creep rupture ductility will be deteriorated at lower stresses as Grade 92.

Similar to the base metal of Opt.G92, the limited creep test results of cross-welds at 650°C also showed moderate enhancement in creep resistance compared to Grade 92 cross-welds. The tests showed type-IV cracking at outer HAZ with a decent area of reduction of $\sim 30\%$. Microstructural analyses indicate that the type-IV cracking is associated with the accumulation of cavities that were related to the amount but not the size of Laves phase formed in the material.

Fracture toughness of the base metal and weldments of Opt.G92 were tested in the transition and ductile regions. The weldments had the reference temperature (T_0) increased to -17°C from -34°C of the base metal, but had greater or comparable toughness in the ductile region at $500\text{--}650^\circ\text{C}$ compared to the base metal.

Acknowledgments

The research was sponsored by the U.S. Department of Energy, under contract number DE-AC05-00OR22725 with Oak Ridge National Laboratory, managed and operated by UT-Battelle, LLC, and under Contract number DE-AC02-06CH11357 with Argonne National Laboratory, managed and operated by UChicago Argonne LLC. Programmatic direction was provided by the Office of Nuclear Energy, Office of Advanced Reactor Technologies.

References

- [1] TANEIKE, et al., “Creep-strengthening of steel at high temperatures using nano-sized carbonitride dispersions”, *Nature* **424** (2003) 294.
- [2] ABE, F., “Analysis of creep rates of tempered martensitic 9%Cr steel based on microstructure evolution”, *Mater. Sci. Eng. A* **510–511** (2009) 64.
- [3] YIN, Y.-F., et al., “Modelling the effects of alloying elements on precipitation in ferritic steels”, *Mater. Sci. Eng. A* **344** (2003) 92.
- [4] HOSOI, Y., et al., “Precipitation behavior of Laves phase and its effect on toughness of 9Cr-2Mo ferritic-martensitic steel, *J. Nucl. Mater.* **141–143** (1986) 461.
- [5] TAN, L., et al., “Microstructure control for high strength 9Cr ferritic-martensitic steels”, *J. Nucl. Mater.* **422** (2012) 45.
- [6] TAN, L., et al., “Effect of thermomechanical treatment on 9Cr ferritic-martensitic steels”, *J. Nucl. Mater.* **441** (2013) 713.
- [7] TAN, L., et al., “Effects of alloying elements and thermomechanical treatment on 9Cr reduced activation ferritic-martensitic (RAFM) steels”, *J. Nucl. Mater.* **442** (2013) S13.
- [8] TAN, L, et al., “Materials procurement and related examinations of advanced ferritic-martensitic and austenitic alloys”, Oak Ridge National Laboratory Report, 2013, ORNL/TM-2013/325.
- [9] TAN, L, et al., “FY14 materials procurements and related examinations of optimized Grade 92 and alloy 709 steels”, Oak Ridge National Laboratory Report, 2014, ORNL/TM-2014/258.
- [10] YAGI, K., et al. [Eds.], “Materials, Subvolume B – Creep Properties of Heat Resistant Steels and Superalloys”, *Landolt-Börnstein Group VIII: Advanced Materials and Technologies, Volume 2*, Springer-Verlag Berlin Heidelberg, 2004.
- [11] NIMS Creep Data Sheet, No. 48A, National Institute for Material Science, Japan, 2012.
- [12] SAMUEL, E.I., et al., “Creep deformation and rupture behavior of P92 steels at 923 K”, *Procedia Eng.* **55** (2013) 64.
- [13] GU, Y., et al., “Investigation of creep damage and cavitation mechanisms in P92 steels”, *Proceedings of the Seventh International Conference on Advances in Materials Technology for Fossil Power Plants*, October 22–25, 2013, Waikoloa, Hawaii, USA.
- [14] PANAIT, C., et al., “Long-term aging effect on the creep strength of the T92 steel”, 9th Liege Conference: Materials for Advanced Power Engineering 2010, Liege, Belgium 2010.

-
- [15] YAGUCHI, M., et al., "Evaluation of long-term creep strength of welded joints of ASME Grades 91, 92 and 122 type steels", Proceedings of the ASME 2012 Pressure Vessels & Piping Conference, July 15-19, 2012, Toronto, Ontario, Canada, PVP2012-78393.